The Bioscan
AN INTERNATIONAL QUARTERLY JOURNAL OF LIFE SCIENCES
20(2): S2: 156-170, 2025 www.thebioscan.com

Synthesis, Characterization, Computational Analysis, and Biological Evaluation of a Novel Tetraaza Macrocyclic Amide Ligand and its Metal Complexes as Potential HDAC-I Inhibitors and Anticancer Agents against Skin Melanoma

P. Yogalakshmi[1]* and **Dr. N. Banumathi[2]**

1*Research Scholar, Reg. No: 19221172032012, Department of Chemistry, Rani Anna Government College for Women
Affiliated to Manonmaniam Sundaranar University, Tirunelveli-12 Tamil Nadu, India.
2 Assistant Professor (Chemistry), Chikkanna Government Arts College, Affiliated to Bharathiar University, Tirupur, 641602, Tamil Nadu, India.
*Corresponding Author: Tel: +91 7845513572, Email:
s.dharu1996@yahoo.com

DOI: 10.63001/tbs.2025.v20.i02.S2.pp156-170

KEYWORDS
Tetra aza ligand,
HDAC1 inhibition,
cytotoxicity,
DFT, docking.

Received on:

12-02-2025

Accepted on:

15-03-2025

Published on:

24-04-2025

ABSTRACT

Objectives: This study aimed to synthesize a tetra aza macrocyclic ligand with Co(II), Ni(II), and Zn II) complexes and explore their antimicrobial, antioxidant, HDAC1 inhibitory, and cytotoxic effects.

Methods: The reaction between diethyl oxalate and o-phenylenediamine produced a tetra aza macrocyclic amide ligand. Its complexes of cobalt (II), nickel (II), and zinc(II) were subsequently prepared by a template synthesis method. Structural confirmation of the ligand and complexes was achieved using elemental analysis, IR, UV–Vis spectroscopy, and molar conductivity measurements.

Findings: The cobalt (II) complex displayed distinctive properties and notable reactivity, highlighted by its broad-spectrum antimicrobial activity and strong binding interactions in molecular docking studies, suggesting promising HDAC1 inhibitory potential. Its high softness indicates increased chemical reactivity, favoring its application in catalysis and charge-transfer processes. In contrast, the zinc (II) complex demonstrated superior cytotoxic activity against A375 melanoma cells. It exhibited antioxidant capacity, positioning it as a strong candidate for therapeutic applications targeting oxidative stress-related conditions.

Novelty: A dual analysis against melanoma cells and HDAC1, using doxorubicin and SAHA as standards, integrates DFT, docking, SwissADME, and ADMET-SAR for a comprehensive therapeutic evaluation.

1.INTRODUCTION

Skin melanoma remains one of the most aggressive, treatment-resistant malignancies, contributing disproportionately to skin cancer-related deaths worldwide [1]. Despite progress in early detection and advanced therapeutic strategies, its incidence continues to rise globally, particularly in fair-skinned populations with high ultraviolet exposure. The advent of targeted therapies such as BRAF and MEK inhibitors and immune checkpoint blockade (ICB) therapies targeting CTLA-4 and PD-1/PD-L1 pathways has revolutionized treatment paradigms, especially for metastatic melanoma. Yet, the challenge of therapeutic resistance, immune evasion, and tumor heterogeneity persists, necessitating the exploration of novel treatment avenues [2].

Among emerging strategies, epigenetic modulation, particularly through histone deacetylase (HDAC) inhibition, has garnered considerable attention. HDACs, which regulate chromatin structure and gene transcription, are implicated in cancer through their ability to repress tumor suppressor genes and facilitate oncogene expression. Dysregulated HDAC activity, especially in Class I isoforms (HDAC1, HDAC2, and HDAC3), contributes to melanoma pathogenesis by promoting immune evasion, angiogenesis, and resistance to apoptosis [3]. Thus, HDAC inhibitors (HDACis) represent a promising therapeutic class with dual actions modulating the immune microenvironment and directly inhibiting cancer cell proliferation.

To date, several HDACis, such as vorinostat and romidepsin, have received FDA approval for hematological malignancies, and

others, like entinostat and panobinostat, are under clinical investigation for solid tumors, including melanoma [4]. Preclinical models demonstrate that HDACis induce cell cycle arrest, differentiation, and apoptosis in melanoma cells while also upregulating major histocompatibility complex (MHC) molecules and tumor associated antigens. Interestingly, HDACis can increase PD-L1 expression, paradoxically enhancing the efficacy of ICB therapies. This synergy positions HDACis as critical agents in combinatorial regimens designed to overcome therapeutic resistance.

Despite these advances, most first-generation HDACis exhibit pan-HDAC inhibition, leading to off-target effects, toxicity, and limited isoform specificity. There is a pressing need for next generation HDACis with improved selectivity, especially toward Class 1 isoforms predominantly involved in melanoma progression [5]. Furthermore, while hydroxamic acids and benzamides dominate the HDACis chemical landscape, novel scaffolds that offer increased stability, binding precision, and pharmacokinetic advantages are urgently needed.

Macrocyclic ligands, particularly tetra aza macrocyclic amide ligands, offer a promising scaffold in this context. These nitrogen containing compounds form kinetically and thermodynamically stable complexes with transition metals such as Co(II), Ni(II), Cu(II), and Zn(II). The incorporation of metal ions not only improves redox activity, lipophilicity, and membrane permeability but also facilitates unique interactions with biological macromolecules inaccessible to the free ligand [6]. Moreover, recent studies highlight their potent antimicrobial, antioxidant, and cytotoxic activities, often surpassing conventional therapeutics.

In drug discovery, computational tools such as Density Functional Theory (DFT) provide insights into molecular reactivity and stability. Additionally, in silico pharmacokinetics and toxicity profiling using platforms like SwissADME and admetSAR enables early filtering of drug-like compounds, conserving time and experimental resources [7].

Yet, a key gap persists in the systematic integration of synthetic chemistry, computational modeling, and comprehensive biological evaluation in the development of HDAC inhibitors, especially macrocyclic scaffolds. Most existing studies either focus solely on computational screening or are limited in vitro assessments without linking structure-activity relationships (SAR) across platforms. There is also a dearth of SAR data connecting metal complexation with enhanced anticancer potency, leaving the mechanistic basis of these enhancements largely unexplored. The present study is designed to address these gaps by synthesizing and characterizing a novel tetraaza macrocyclic amide ligand and its Co(II), Ni(II), Cu(II), and Zn(II) complexes. This will be followed by rigorous DFT and docking analyses targeting HDAC1, coupled with SwissADME and admetSAR based pharmacokinetic profiling. Biological evaluations will span antimicrobial, antioxidant, and cytotoxic assays, including apoptosis induction in melanoma cell lines. To our knowledge, this is among the first holistic studies integrating such a spectrum of synthetic, computational, and biological methodologies focused specifically on HDAC-I inhibition in melanoma.

By introducing novel chemical entities and validating their potential across computational and biological domains, this work not only enhances our understanding of HDACis but also contributes meaningfully to the translational drug discovery pipeline. The findings are expected to pave the way for more selective, potent, and clinically viable HDAC-targeted therapies, especially for refractory and metastatic melanoma.

2.METHODOLOGY

All reagents and solvents were analytical grade and used without further purification. Diethyl oxalate, o-phenylenediamine, and metal salts ($CoCl_2 \cdot 6H_2O$, $NiCl_2 \cdot 6H_2O$, $ZnCl_2$) were procured from E. Merck. Conductivity was measured in dry EMF using a Model 601 conductivity bridge. Melting points were determined using an electrical melting point apparatus. UV-visible diffuse reflectance spectra were recorded at room temperature with a Jasco V750 spectrophotometer, and FT-IR spectra were captured using FT-IR Spectrophotometer-Shimadzu, Model: IR Affinity-I.

2.1. Synthesis of macrocyclic ligand (2oxap): (5,8,13,16-tetrahydrodibenzo[b,h][1,4,7,10]tetraazacyclododecine 6,7,14,15-tetrone, $C_{16}H_{12}N_4O_4$)

The macrocyclic ligand 5,8,13,16-tetrahydrodibenzo[b,h] [1,4,7,10]tetraaza cyclododecine-6,7,14,15-tetrone ($C_{16}H_{12}N_4O_4$) was synthesized via the condensation of diethyl oxalate (2.7 mL, 0.02 mol) and o-phenylenediamine (2.162 g, 0.02 mmol) in the presence of concentrated hydrochloric acid (1 mL). Diethyl oxalate was first heated with HCl for 2 hours, cooled in an ice bath, and then brought to room temperature before adding o-phenylenediamine dissolved in ethanol. A white precipitate formed, which was refrigerated for 4 hours, then filtered and washed with THF, diethyl ether, and petroleum ether. Owing to the low yield obtained during the ligand synthesis, a template synthesis approach was employed for the preparation of its corresponding metal complexes. Figure 1 shows a synthetic route for tetra aza macrocyclic amide ligand.

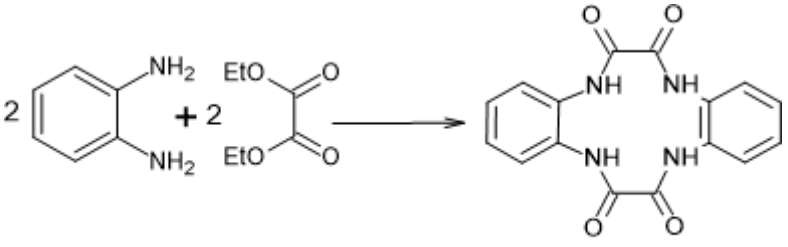

Figure 1. Synthesis of Ligand

2.2. Synthesis of Complexes (2oxapCo, 2oxapNi and 2oxapZn): $[Co(C_{16}H_{12}N_4O_4)\ Cl_2]$, $[Ni(C_{16}H_{12}N_4O_4)]\ Cl_2$ and $[Zn(C_{16}H_{12}N_4O_4)]\ Cl_2$

A hot ethanolic solution of diethyl oxalate (2.7 mL, 0.02 mol) was mixed with a hot o-phenylenediamine solution (2.162 g, 0.02 mol), and the mixture was refluxed. An equimolar ethanolic solution of a metal chloride (dry $ZnCl_2$/$NiCl_2 \cdot 6H_2O$/$CoCl_2 \cdot 6H_2O$) was gradually added while being constantly stirred during reflux. After refluxing the reaction mixture for an hour, a colorful precipitate was produced. This precipitate was filtered and repeatedly washed with petroleum ether, ethanol, THF, and diethyl ether [8].

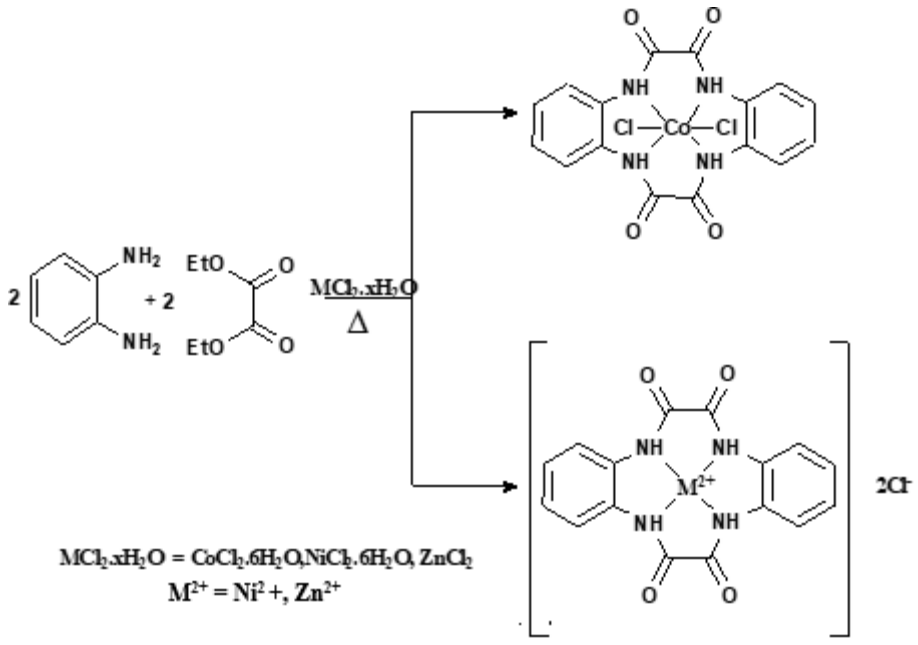

Figure 2. synthetic route for tetra aza macrocyclic amide complexes

2.3. Preliminary Test for Water Molecule and Chloride Ion

The presence of water in the crystallized metal complexes was assessed using cobalt chloride paper. No distinct color change from blue to pink confirmed the absence of water molecules within the crystalline structure. Additionally, to identify the existence of uncoordinated chloride ions (those not involved in coordination with the metal center), aqueous silver nitrate ($AgNO_3$) and ammonium hydroxide (NH_4OH) were introduced into the complex solutions. The immediate formation of a white precipitate, which subsequently dissolved upon the addition of excess NH_4OH, confirmed the presence of free chloride ions outside the coordination sphere [9].

2.4. ADMET analysis

The pharmacokinetic behavior of the synthesized drug candidates was evaluated using the Swiss ADME server (http://www.swissadme.ch/), which predicts key properties such as absorption, distribution, metabolism, and excretion (ADME). SMILES representations of the compounds were input to assess their drug-likeness. Additionally, potential toxicity was predicted using the admits server (https://lmmd.ecust.edu.cn/admetsar2) to support the safety profile of the compounds.

2.5. In silico molecular docking studies

2.5.1. Retrieval of the tertiary structure of protein and structure validation

To identify the target protein of synthesized compounds, the SMILES representation of the ligand was derived from its 3D structure and submitted to the Therapeutic Target Database (TTD). The corresponding protein target was then identified using the UniProt server, and the relevant PDB ID was obtained. Specifically, the 3D structure of the HDAC-I enzyme (PDB ID: 4BKX), complexed with the ELM2-SANT domain of MTA1 from the NuRD complex, was retrieved from the RCSB Protein Data Bank. The structure, stored in PDB format, was first subjected to energy minimization using Swiss-PDB Viewer (Swiss-PDB Viewer 4.1.0) to refine atomic positions and improve structural geometry. Its quality was then assessed using a Ramachandran plot generated via the PDBsum server. (https://www.ebi.ac.uk/thornton-srv/databases/pdbsum/). Additionally, the ProSA server (https://prosa.services.came.sbg.ac.at/prosa.phpk/thornton-srv/databases/pdbsum/). was used to assess the protein's overall structural quality through Z-score analysis, determining the model's reliability for further studies.

2.5.2. Binding pocket prediction

Protein active sites were predicted using the machine learning-based Prank web server (https://prankweb.cz/). A binding site is a specialized region of an enzyme or protein that allows it to connect with specific molecules and accelerates biological events.

2.5.3. Ligand designing and preparation

The synthesized compounds were structurally optimized for molecular docking and stored in PDB format to investigate their potential interactions with the target enzyme.

2.5.4 Molecular Docking Analysis

To evaluate the anticancer potential of synthesized compounds targeting the HDAC-1 enzyme, molecular docking was performed in comparison with the approved drug SAHA. The HDAC-1 receptor protein, comprising chains A and B, chain B was selected, and it was prepared by removing water molecules and small ions, except for the zinc ion due to its structural and functional role. Polar hydrogen atoms were added to adjust tautomeric and oxidation states. Docking was conducted using AutoDock Vina (version 1.5.6), which enables flexible ligand docking. The molecular interactions, including both 2D and 3D views, were analyzed using Biovia Discovery Studio Visualizer to assess the binding between the HDAC-1 receptor and the synthesized as well as approved compound.

2.6. DFT Studies

To optimize the structures of the macrocyclic ligand (2oxap) and its Co(II), Ni(II), and Zn(II) complexes without symmetry constraints, Density Functional Theory (DFT) simulations were performed. The geometry optimization utilized Gaussian 16 (Revision C.02) with the B3LYP functional. The LANL2DZ basis set was applied for metal atoms, while the 6-311++G (d,p) basis set was used for C, H, O, and N atoms. GaussView 6.0 was used to visualize the optimized structures. Molecular Electrostatic Potential (MEP) analysis was carried out to determine the electron density distribution and possible reactive sites, and important electronic parameters like total energy, HOMO, and LUMO energies were computed.

2.7. Antimicrobial studies

2.7.1. Antibacterial essay

The antibacterial activity of 10 mg/mL test samples was evaluated using the well diffusion method on nutrient agar against *E. coli* and *S. aureus*. After inoculating the agar plates with bacterial cultures, wells were filled with varying volumes (25–100 µL) of the test solution. Plates were incubated at 37°C for 24 hours, and zones of inhibition were measured. Tests were

conducted in triplicate, with chloramphenicol serving as the positive control.

2.7.2. Antifungal studies

The antifungal activity of 10 mg/mL test samples was assessed via the well diffusion method on YPD agar against *Candida albicans*. Plates were inoculated with fungal suspension, and wells were filled with 25–100 µL of the test solution. After incubation, zones of inhibition were measured. Tests were done in triplicate, with fluconazole as the positive control.

2.8. Antioxidant studies

The antioxidant potential of the test samples was determined using the DPPH free radical scavenging assay. Various concentrations (10–50 µg/mL) of the samples were mixed with 0.1 mM DPPH solution and incubated at room temperature for 30 minutes. Absorbance was recorded at 517 nm. L-ascorbic acid (10–500 µg/mL) served as the positive control. The scavenging activity was calculated using the formula Scavenging effect (%) = $(A_c - A_t) / A_c \times 100$, Where A_c = absorbance of control, A_t = absorbance of the test sample.

2.9. Cytotoxic studies

PASS CLC Pred (http://www.way2drug.com/Cell-line/), analysis indicated strong cytotoxic activity of the tetra aza macrocyclic amide ligand against skin melanoma and glioma cell lines, highlighting its potential selectivity and therapeutic promise for skin-related cancers.

The cytotoxicity of the tetra aza macrocyclic ligand and its metal complexes was assessed on A375 cells using the MTT assay. Cells were seeded at 50,000 cells/well in 96-well plates and incubated for 24 hours before treatment with various concentrations of test compounds. After another 24-hour incubation, MTT was added and incubated for 4 hours. Formazan crystals were dissolved in DMSO, and absorbance was measured at 570 nm. Growth inhibition was calculated as

% Inhibition = [(OD of Control – OD of Sample) / OD of Control] × 100

IC_{50} values were determined using nonlinear regression analysis with GraphPad Prism.

2.10. Apoptosis studies by AO-EB Dual Fluorescent Staining Method

The AO-EB dual staining technique distinguishes viable, apoptotic, and necrotic cells based on fluorescence and morphology. Acridine Orange stains all nuclei green, while Ethidium Bromide marks membrane compromised cells with orange/red fluorescence. This method highlights apoptosis indicators like chromatin condensation and membrane blebbing, aiding in the assessment of drug-induced cell death.

3.RESULTS AND DISCUSSION

3.1. Characterization of synthesized compounds

The analytical data presented in Table 1 indicates that the reaction of diethyl oxalate with o-phenylenediamine produces the ligand 2oxap(2O). Macrocyclic complexes of Cobalt(II), Nickel(II), and Zinc(II) were synthesized via a template method using a 1:1 molar ratio in ethanolic solution, resulting in the respective complexes: 2oxapCo(2OC), 2oxapNi(2ON), and 2oxapZn(2OZ). Both the macrocyclic ligand and its metal complexes exhibit solubility in DMF and DMSO. Spectral analyses, including infrared (FT-IR), electronic spectra, and molar conductance data, are presented in Table 2.

Compound / formula	Molecular weight	Color	M. Point °C	Yield %	Elemental analysis Calculated (experimental)			
					C	H	N	Cl
2oxap (2O) $C_{16}H_{12}N_4O_4$	324.29	white	140	20	59.26 (59.20)	3.73 (3.71)	17.28 (17.25)	-
$[Co(2oxap)Cl_2]$ (2oxapCo) $[Co(C_{16}H_{12}N_4O_4)\ Cl_2]$	452.96	brown	>250	85	42.32 (42.30)	2.66 (2.65)	12.34 (12.33)	15.61 (15.58)
$[Ni(2oxap)]Cl_2$ (2oxapNi) $[Ni(C_{16}H_{12}N_4O_4)]\ Cl_2$	451.96	violet	>250	90	42.34 (42.32)	2.66 (2.65)	12.34 (12.32)	15.62 (15.58)
$[Zn(2oxap)]Cl_2$ (2oxapZn) $[Zn(C_{16}H_{12}N_4O_4)]\ Cl_2$	457.95	cream	150	60	41.72 (41.63)	2.63 (2.53)	12.16 (12.14)	15.39 (15.35)

Table 1. The analytical data and physical properties of the synthesized compounds

Comp	$\sqrt{}_{N-H}$ (cm^{-1})	Amide (cm^{-1})				$\gamma_{(M-N)}$ (cm^{-1})	Molar conductivity S cm^{-1} mol^{-1}	Λ nm
		I γ(C=O)	II γ(C-N) + δ (N-H)	III δ(N-H)	IV Φ(C=O)			
2oxap	3340	1666	1558	1319	748	-	-	234 297
2oxapCo	3294	1682	1504	1327	740	478	18	234 296 342 394 488
2oxapNi	3286	1687	1504	1327	748	478	100	213 260 302 547
2ocapZn	3294	1681	1504	1327	756	479	111	260 293 435

Table 2 The IR, electronic spectral data and molar conductance measurements of the synthesized compounds

The coordination behavior and geometry of the ligand 2oxap and its Co(II), Ni(II), and Zn(II) complexes were investigated through IR, UV-visible spectroscopy, molar conductivity measurements and silver nitrate test.

The IR spectra of the ligand lack characteristic bands at 1700 cm^{-1} (γC=O), 3380 cm^{-1} (γ_{as} NH_2), and 3250 cm^{-1} (γ_s NH_2), corresponding to the carbonyl group and free primary amine. This absence suggests successful condensation between the amino and keto groups [10]. In contrast, the IR spectra of the resulting metal complexes display these absorptions at altered frequencies, indicative of ligand coordination. Notably, the N–H and amide-II stretching frequencies shift downward by approximately 50–60 cm^{-1} and 50–55 cm^{-1}, respectively. Meanwhile, the C=O stretching band shifts upward by 10–20 cm^{-1}, suggesting that the amide oxygen does not participate in coordination [11]. These spectral changes support the involvement of amide nitrogen atoms in coordination with metal ions. Further confirmation comes from the emergence of new bands in the 439–478 cm^{-1} range in all complex spectra, attributable to ν(M-N) vibrations.

The UV-Vis (diffuse reflectance) spectroscopy of the complexes was carried out and recorded in wavelength (nm). Electronic spectral analysis provided insight into the geometry of the complexes. The Co(II) complex displayed absorption bands at 234nm, 296nm, 342 nm, and 394 nm, the last one corresponding to d–d transitions ($^4T_{1g}(F) \rightarrow {}^4A_{2g}(F)$) typical of a high-spin octahedral geometry [12].

The Ni (II) complex showed transitions at 213, 260, 302, and 547 nm, the last one corresponding to d-d transition ($^1A_{1g} \rightarrow {}^1B_{1g}$) consistent with a square planar geometry [13]. The Zn (II) complex, being a d^{10} system, exhibited no d–d transitions but showed prominent bands at 250nm, 293nm, and 435 nm, attributed to LMCT and intra-ligand transitions, confirming a tetrahedral geometry.

Molar conductivity measurements in DMF (10^{-3} M) further corroborated the proposed structural assignments. The Co(II) complex exhibited a low conductivity value, indicative of a non-electrolyte, suggesting the formation of a neutral six-coordinate species in solution. In contrast, the Ni(II) and Zn(II) complexes showed significantly higher conductivity values, consistent with 1:2 electrolyte behavior. This was further supported by positive chloride ion detection using silver nitrate and ammonium hydroxide, confirming the presence of two dissociated chloride counterions in the solution.

3.2. In Silico admet studies

The synthesized compounds, evaluated using SwissADME and admetSAR tools, demonstrate promising characteristics for drug development.

The synthesized compounds and reference drug SAHA showed strong drug-likeness, complying with Lipinski's Rule of Five, with bioavailability scores of 0.55, no PAINS alerts, and feasible synthetic accessibility (2.76–3.95) [14]. 2oxap, 2oxapCo, and SAHA demonstrated positive Log P values, favoring oral and dermal delivery, while 2oxapNi and 2oxapZn, being more hydrophilic, may be better suited for injectable use with extended circulation [15].

All synthesized compounds were non-AMES toxic and non-carcinogenic, suggesting a safer profile than SAHA. Although Caco-2 permeability was low across all compounds, systemic absorption remains acceptable [16]. 2oxap, 2oxapCo, and SAHA showed high gastrointestinal absorption, making them viable for oral administration, while 2oxapNi and 2oxapZn showed low GIA. None of the compounds cross the blood-brain barrier, reducing CNS-related risks. 2oxap and SAHA are not P-gp substrates, favoring drug retention, whereas metal complexes are substrates, potentially aiding targeted distribution [17]. All compounds exhibited low skin permeability, making them unsuitable for transdermal delivery.

Notably, 2oxapCo, due to the presence of Co(II), may bind the Zn^{2+}-dependent HDAC-1 active site through metal coordination and hydrogen bonding, offering a dual inhibitory mechanism and improved target specificity, a strategy consistent with epigenetic drug design for metalloenzymes [18].

3.3. In silico molecular docking studies

A comparative molecular docking analysis was performed to evaluate the binding affinities and interaction profiles of 2oxap and its metal derivatives, namely 2oxapCo, 2oxapNi, and

2oxapZn, and SAHA as an HDAC-1 inhibitor, using AutoDock Vina with the HDAC-1 crystal structure (PDB ID: 4BKX).
The results confirmed that the binding energy of the compounds with the receptor decreased upon coordination. Among the compounds tested, 2oxapZn exhibited the highest binding energy (-7.3 kJ/mol), followed closely by 2oxapCo (-7.2 kJ/mol). However, 2oxapZn presented an unfavorable electrostatic clash with HIS178, potentially compromising its binding stability and biocompatibility (Table 4).

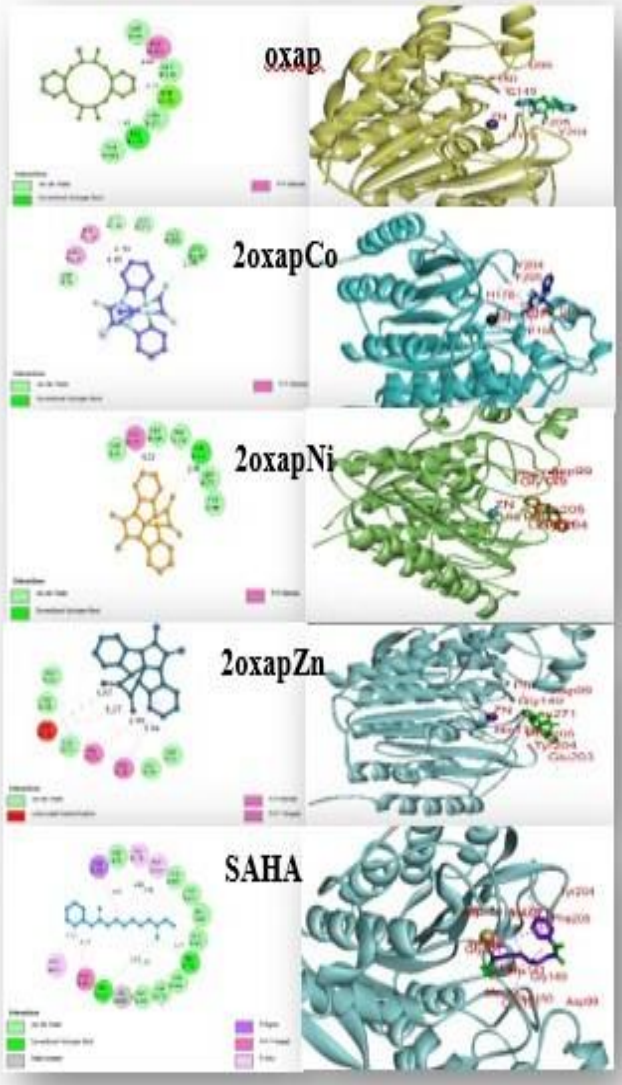

Figure 3. The 2D (left) and 3D (right) docking poses of the synthesized compounds with the receptor 4BKX

In contrast, 2oxapCo demonstrated a highly favorable interaction profile, forming a conventional hydrogen bond with HIS178 and π-π stacking interactions with both PHE150 and PHE205. Its Van der Waals interactions with ASP99, GLY149, LEU271, and TYR204 were specific and compact, enhancing its structural compatibility with the HDAC-1 binding site. Notably, 2oxapCo lacked any destabilizing interactions, unlike its Zn analog, and outperformed SAHA, which had a weaker binding affinity (-6.3 kJ/mol) and fewer targeted interactions, as shown in Figure 3.
The combination of high binding affinity, well-oriented interactions, and the absence of unfavorable contacts positions 2oxapCo as a promising lead compound for further development in epigenetic cancer therapy. Its profile supports continued investigation into metal coordinated HDAC inhibitors with improved isoform selectivity and pharmacokinetic properties [19].

3.4. DFT studies

This study presents a comprehensive Density Functional Theory (DFT) analysis of tetra aza macrocyclic amide-based ligand and its transition metal complexes. Ground state geometries were optimized in the gas phase without geometrical constraints using Gaussian 16, Revision C.02, with visualization performed via GaussView 6.0. The B3LYP functional with a 6-311++G(d,p) basis set was employed for the free ligand 2oxap, while LANL2DZ was used for cobalt(II), nickel(II), and zinc(II) complexes. Electronic structures, including the HOMO-LUMO gap, molecular electrostatic potential (MEP), and global chemical reactivity descriptors, were evaluated to elucidate the electronic behavior and stability of the compounds. The optimized structures (Figure 4) and the energy gap between HOMO-LUMO of the orbital The HOMO and LUMO energies were utilized to calculate several chemical reactivity descriptors, including the bandgap (ΔE), ionization potential (IP), electron affinity (EA), electronegativity (x), chemical potential (μ), hardness (η), softness (S), electrophilicity index (ω), and nucleophilicity index (N), which are summarized in Table 3. These parameters provide critical insights into the reactivity and stability of the synthesized compounds.

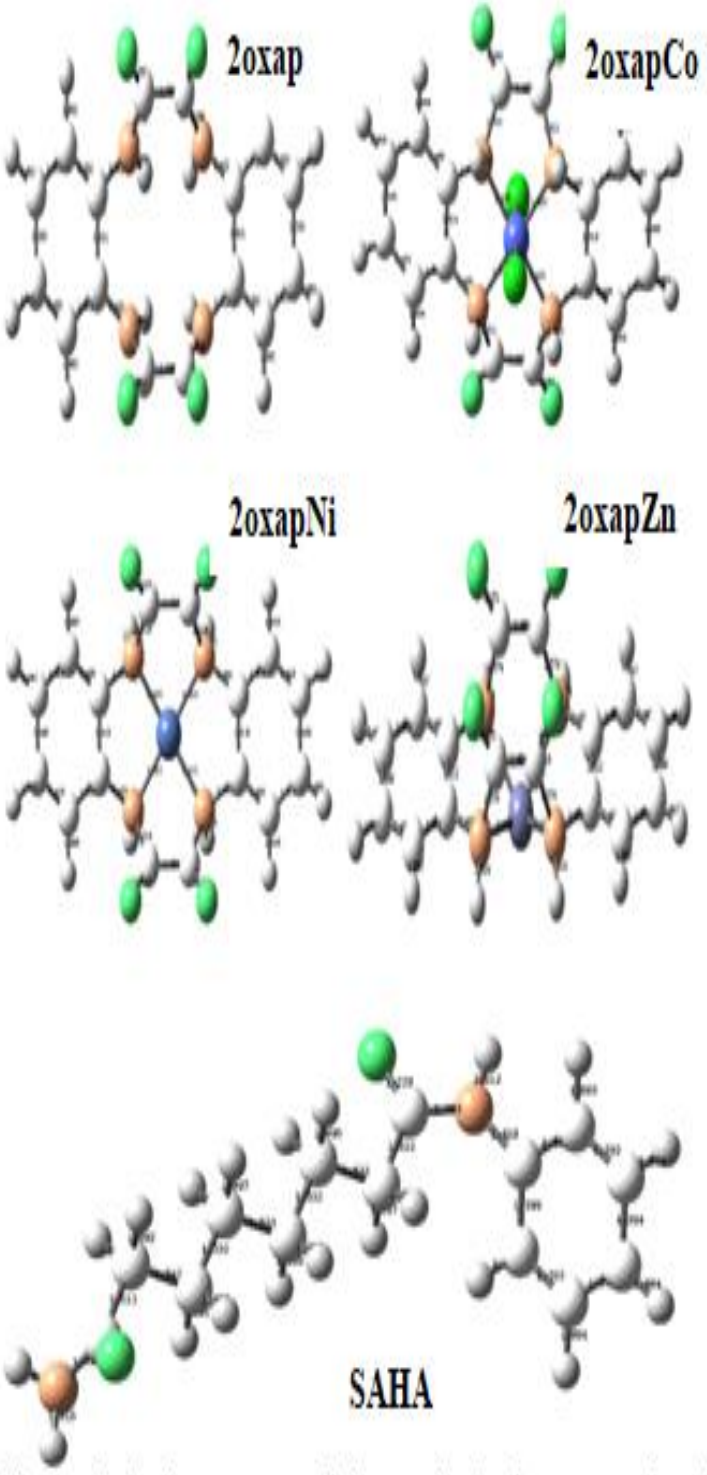

Figure 4. The optimized geometry of the synthesized compounds utilizing B3LYP/ LANL2DZ/ 6311++G(d,p) level of calculation

Comp	2oxap	2oxapCo	2oxapNi	2oxapZn	SAHA
Energy (a.u)	-1137.1359	-1311.7005	-1305.3633	-1202.1833	-880.9455
Dipolemoment (μ)	8.4977	4.8531	8.3308	14.5025	2.5246
$E_{HOMO\ (Hartree)}$	-0.26611	-0.17947	-0.51823	-0.15320	-0.24345
$E_{LUMO\ (Hartree)}$	-0.08110	-0.15016	-0.40597	-0.09490	-0.03592
$E_{HOMO\ (eV)}$	-7.2412	-4.8836	-14.1018	-4.1688	-6.6246
$E_{LUMO\ (eV)}$	-2.2068	-4.08606	-11.0470	-2.5824	-0.9774
Bandgap (ΔE)	5.0344	0.7975	3.05479	1.5864	5.6472
IP (eV)	7.2412	4.8836	14.1018	4.1688	6.6246
EA (eV)	2.2068	4.08606	11.0470	2.5824	0.9774
Electro Negativity (χ) (eV)	4.724	4.4848	12.5744	3.5256	3.8010
Chemical potential (μ) (eV)	-4.724	-4.4848	-12.5744	-3.5256	-3.8010
Chemical hardness (η) (eV)	2.5172	0.3988	1.5274	0.7932	2.8236
Global softness (S) (eV^{-1})	0.1986	1.2538	0.3273	0.6304	0.1771
Electrophilicity index (ω) (eV)	1.2586	0.1994	0.7637	0.3966	1.4118
nucleophilicity index (N)	0.7945	5.0150	1.3094	2.5214	0.7083

Table 3. The predicted quantum chemical descriptors for the synthesized compounds and reference compound

The binding energy values revealed that 2oxapCo forms the most stable complex, while SAHA exhibited the lowest stability among the compounds studied. The stability order based on binding energy was as follows:

SAHA < 2oxap < 2oxapZn < 2oxapNi < 2oxapCo

Dipole moment analysis indicated that the 2oxapCo complex possesses the highest molecular symmetry, whereas 2oxapZn demonstrated the least, reflected by its high dipole moment [20]. Notably, a decrease in the HOMO–LUMO energy gap was observed upon complexation of the ligand with transition metals, shown in Figure 5, indicating increased chemical reactivity and reduced kinetic stability due to enhanced polarizability and charge transfer [21].

Moreover, the negative values of chemical potential across all metal complexes confirmed their thermodynamic stability. Among these, 2oxapNi showed lower chemical potential and higher electronegativity, implying its relatively electrophilic character, Lewis acid, and lower anticipated biological activity. According to the Hard and Soft Acids and Bases (HSAB) theory, the metal complexes, characterized by reduced hardness and increased softness post-complexation, are more compatible with soft biological targets such as proteins and cell membranes, indicating a propensity for improved biological activity [22].

The electrophilicity index decreased upon complexation, with 2oxapCo exhibiting the lowest value, suggesting reduced toxicity and enhanced biological compatibility. Simultaneously, the nucleophilicity index was highest for 2oxapCo, supporting its potential as the most biologically active compound among the synthesized compounds.

These findings underline the importance of quantum chemical descriptors in predicting the behaviour and potential bioactivity of novel metal complexes, contributing valuable insight into the design of new therapeutically relevant compound.

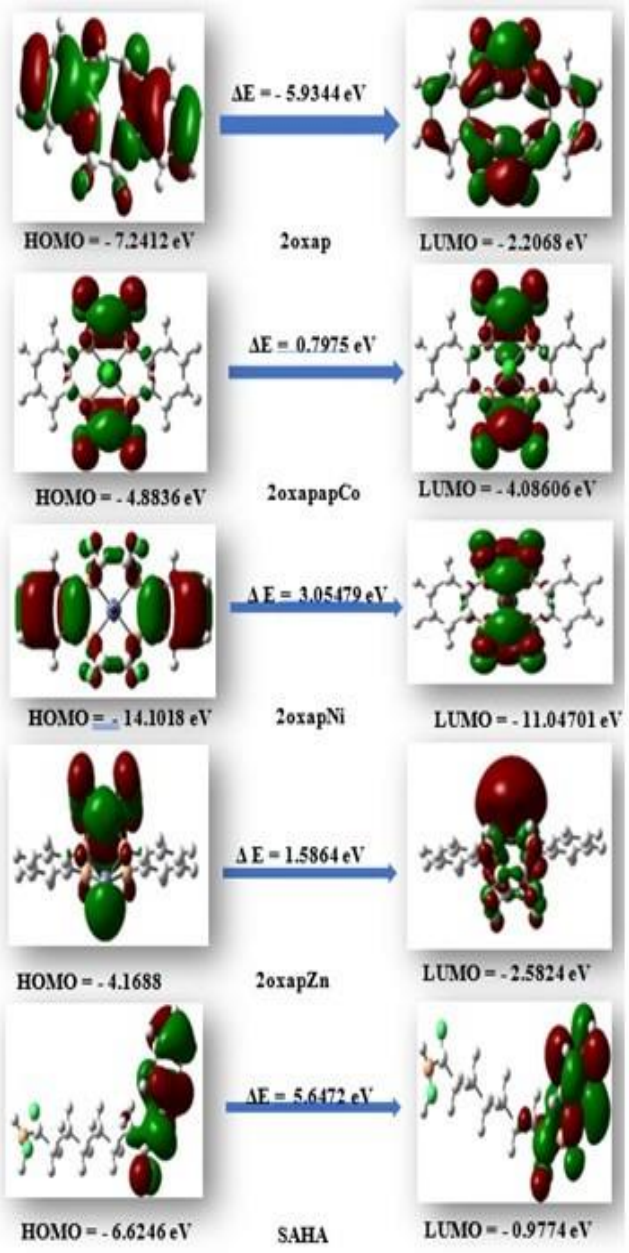

Figure 5. The frontier molecular orbitals of the synthesized compounds calculated from DFT approach

3.5. Molecular electrostatic potential maps

The Molecular Electrostatic Potential (MESP) is a powerful analytical tool that concurrently reveals a molecule's size, shape, and distribution of electrostatic potential, distinguished by color to indicate positive, negative, and neutral regions. It is instrumental in elucidating the link between molecular structure and physicochemical behavior.

The MESP map highlights reactive sites: red areas indicate nucleophilic (electron-rich) zones, blue indicates electrophilic (electron-deficient) regions, and green indicates neutral potential. In the synthesized molecules illustrated in Figure 6, red and yellow regions mark areas amenable to electrophilic attack, while the blue region is prone to nucleophilic attack. The gradient of electrostatic potential is represented in the order: red < orange < yellow green < blue [23].

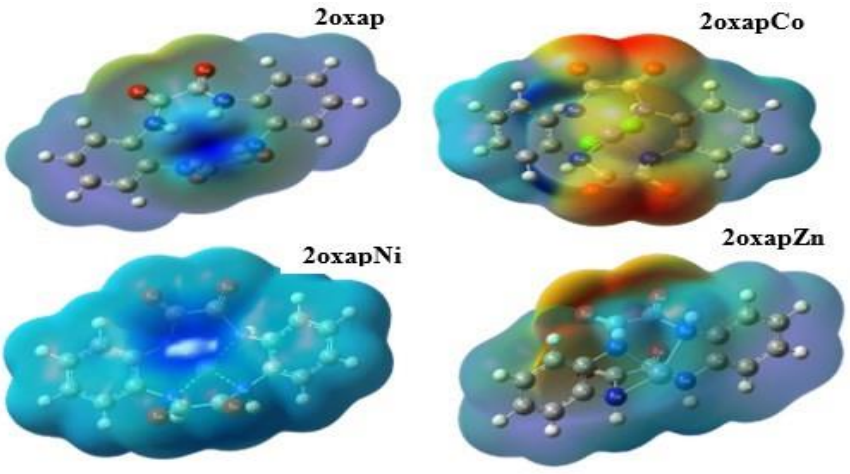

Figure 6. The Molecular Electrostatic potential of the synthesized compounds from DFT approach

3.6. Antimicrobial activities

Table 5 presents the results of antibacterial and antifungal studies conducted on the synthesized compounds (2oxap, 2oxapCo, 2oxapNi, and 2oxapZn) and compares them with standard drugs chloramphenicol and fluconazole. The effectiveness of each compound was evaluated based on the diameter of the inhibition zone (in mm) (Figure 7), which reflects the compound's ability to inhibit microbial growth at different concentrations (25, 50, 75, and 100 µg/mL).

All compounds demonstrated increased antimicrobial activity with rising concentrations. The 2oxapCo complex exhibited the highest antibacterial and antifungal activity, notably surpassing fluconazole against C. albicans. The 2oxapNi complex showed moderate activity against E. coli and S. aureus at the highest concentration. The 2oxapZn complex displayed weak or negligible activity, with a maximum inhibition only against S. aureus.

Metal complexes exhibit antimicrobial activity through multiple mechanisms, namely enhanced membrane permeability due to increased lipophilicity; interference with DNA, enzymes, and ribosomes; generation of reactive oxygen species (ROS) leading to oxidative damage; and metal ion toxicity disrupting essential microbial functions[24]

s.no.	compound	Binding energy kJ / mol From Autodock vina using 4bkxbspdb. pdbqt file	Conventional Hydrogen bond	pi-pi stacked	pi-pi T-stacked	Vande rwaals	pi-alkyl	Metal-acceptor	Unfavourable Positive-positive interaction	Pi-sigma
1	2oxap	-6.5	HIS178	PHE 150 PHE 205	-	ASP 99, GLY 149, LEU 271, TYR 204	-	-	-	-
2	2oxapCo	-7.2	HIS178	PHE 150 PHE 205	-	ASP 99, GLY 149, LEU 271, TYR 204	-	-	-	-
3	2oxapNi	-6.7	HIS178	PHE 205	-	ASP 99, GLY 149, PHE150, LEU 271, TYR 204	-	-	-	-
4	2oxapZn	-7.3	-	PHE 150 PHE 205	HIS 178	ASP 99, GLY 149, PHE 150, GLU 203, TYR 204, LEU 271	-	-	HIS 178	-
5	SAHA	-6.3	HIS141, HIS142	-	TYR 204	MET 30, ASP 99, GLY 149, CYS 151, ASP 264, ASP 176, GLY 301, TYR 303	PHE 150, HIS 178, LEU 271	Zn 600	-	PHE 205

Table 4: The binding energy and interactions of synthesized compounds with Receptor (4BKX)

S.No.	Comp.	Concentration	Zone of inhibition (diameter in mm)		
			Antibacterial studies		Antifungal studies
			S.aureus	*E.coli*	*C.albicans*
1	2oxap	25	10	9	8
		50	12	11	14
		75	16	16	17
		100	20	19	18
2	2oxapCo	25	15	16	18
		50	17	18	20
		75	20	21	23
		100	22	22	25
3	2oxapNi	25	-	8	-
		50	11	12	10
		75	13	15	11
		100	15	18	13
4	2oxapZn	25	-	-	-
		50	-	-	-
		75	-	-	-
		100	9	8	-
5.	Chloramphenicol	100	20	20	-
	Fluconazole	100	-	-	21

Table 5. The antimicrobial activities (ZOI in mm) of the synthesized compounds

Cobalt(II) forms stable complexes, enhancing membrane permeability and reactive oxygen species (ROS) generation due to its strong redox potential [25]. The most broad-spectrum antimicrobial action is seen by 2oxapCo, which also exhibits reduced electrophilicity and increased nucleophilicity. When compared to other drugs, these properties imply superior biological activity and potentially a lower toxicity profile.

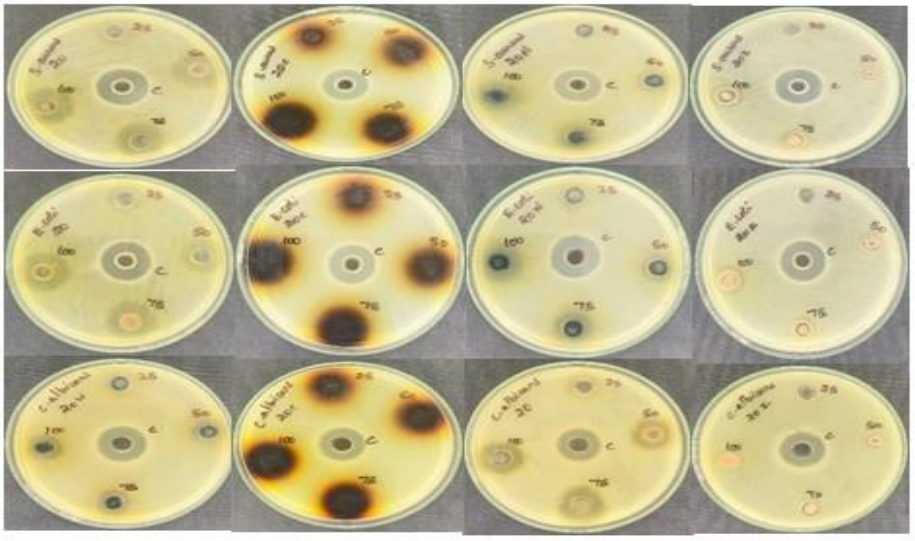

Figure 7. The Antimicrobial Activities (ZOI in mm) of the synthesized compounds

3.7. Antioxidant Activity

The DPPH (2,2-diphenyl-1-picrylhydrazyl) free radical scavenging assay, is a standard method used to evaluate the antioxidant potential of compounds. The study compares the antioxidant activity of four samples 2oxap, 2oxapCo, 2oxapNi, and 2oxapZn at varying concentrations (10 to 50 µg/mL), with ascorbic acid serving as the positive control.

All samples exhibited an increase in DPPH scavenging activity as the concentration increased from 10 to 50 µg/mL, indicating dose-dependent antioxidant behavior. Results showed that while all tested compounds exhibited antioxidant activity, they were less effective than ascorbic acid. Among the complexes, 2oxapZn demonstrated the highest dose-dependent activity, whereas 2oxapNi had the weakest, as shown in Figure 8. Overall, the complexes enhanced the ligand's scavenging ability, suggesting their potential to protect against oxidative damage. The human body utilizes enzymatic and non-enzymatic antioxidants to combat damage from free radicals, which are linked to diseases like cancer, cardiovascular, and neurological disorders [26].

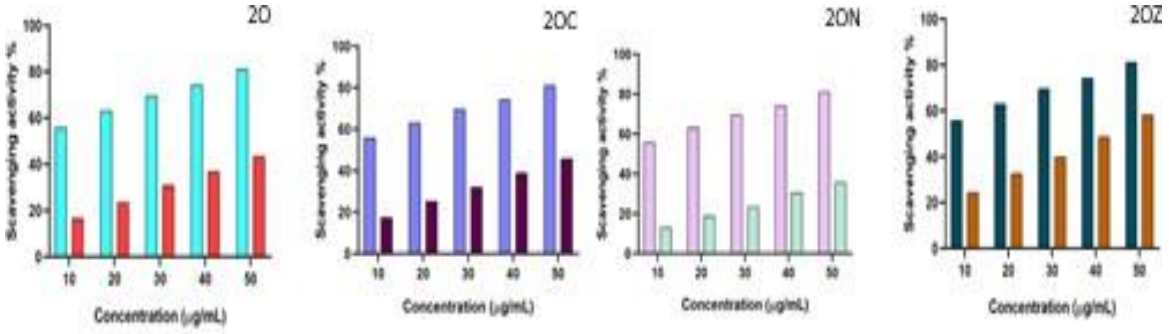

Figure 8. The graphical representation of antioxidant activity of the synthesized compound

3.8. in vitro cytotoxicity studies

A375 cells were treated with the samples 2oxap, 2oxapCo, 2oxapNi, and 2oxapZn at concentrations of 7.81, 15.62, 31.25, 62.5, 125, 250, and 500 µg/mL. After 24 hours of treatment, an MTT assay was performed, and the results were analyzed using GraphPad Prism software [27]. The results indicate that all four samples exhibited significant inhibition of A375 cells, as shown in Table 6. Among them, the 2oxapZn and 2oxap samples demonstrated the highest half-maximal inhibitory concentrations, measuring 9.24 µg/mL and 9.35 µg/mL, respectively, as represented in Figure 9.

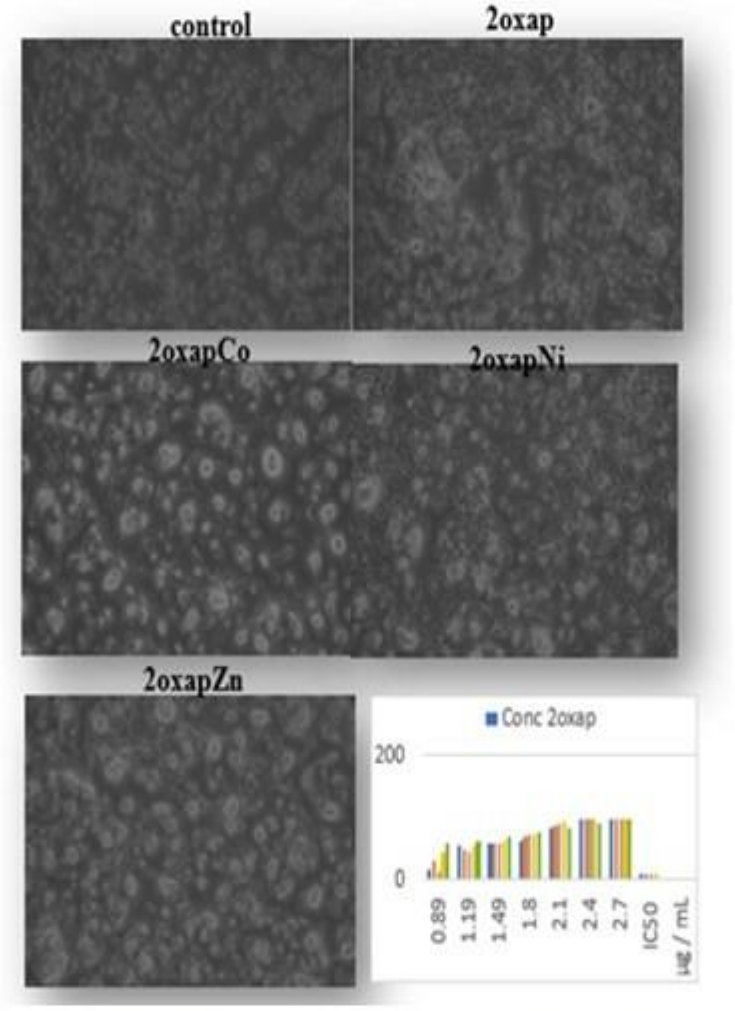

Figure 9. Pictorial and graphical representation of synthesized compounds and the control obtained through MTT assay against A 375 melonama cancer cell line.

3.9. Apoptosis of Dual Staining

A375 cells were treated with the compounds 2oxap, 2oxapCo, 2oxapNi, and 2oxapZn at concentrations of 125 µg/mL and

62µg/mL. After 24 hrs of treatment. Cells were stained with 100µL of acridine orange and Ethidium bromide (1:1) at the concentration of 20µg/mL. After staining, the cells were visualized under a fluorescent microscope. Apoptosis was observed in all four samples at 125 µg/mL [28]. Compared to the control, treated samples have shown the staining of red color dots around the cells represented in Figure 10, and the compound 2oxapZn has shown the maximum effect.

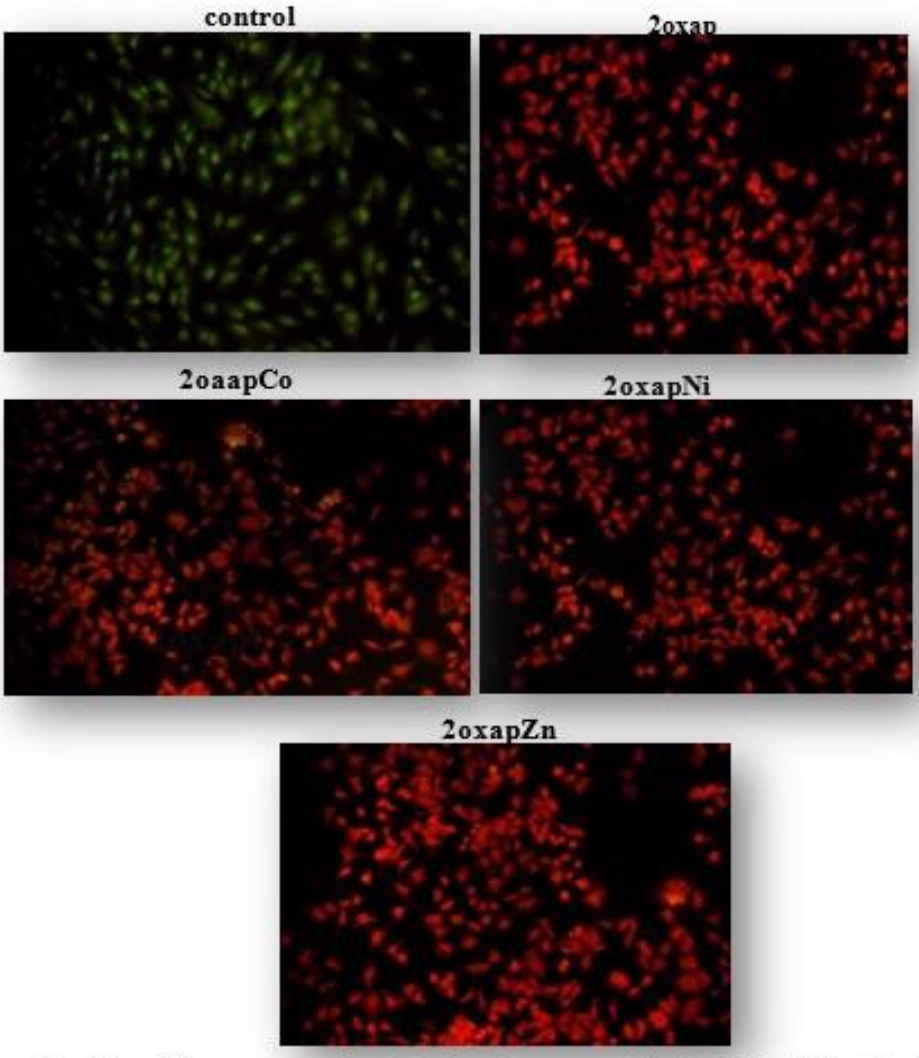

Figure 10. Pictorial representation of induced apoptosis in A 375 cell line by AO-EB staining method with the synthesized compounds at the concentration of 125µg/mL

4.CONCLUSION

A novel tetra aza macrocyclic amide ligand (2oxap) and its transition metal complexes with Co(II), Ni(II), and Zn(II) were successfully synthesized and structurally characterized through IR, UV, conductivity data, and chloride ion test, revealing distinct geometries: octahedral (Co), square planar (Ni), and tetrahedral (Zn). Integrated in silico, DFT, and in vitro studies demonstrated that all complexes exhibit favourable drug-likeness and safety profiles.

Among the compounds, 2oxapCo stood out as the most promising candidate, demonstrating favorable pharmacokinetics, strong HDAC-1 binding affinity, excellent broad-spectrum antimicrobial activities, stable geometry, and significant biological potential as indicated by quantum chemical descriptors. Conversely, 2oxapZn exhibited the highest antioxidant activity and potent cytotoxicity against A375 melanoma cells, highlighting its dual capacity to modulate oxidative stress and inhibit cancer cell growth, despite its comparatively lower docking stability.

Collectively, the study highlights the therapeutic potential of these metal complexes, particularly 2oxapCo as a lead compound for epigenetic cancer therapy and antimicrobial drug development, and 2oxapZn for its cytotoxic and antioxidant properties.

5.REFERENCES

- Raucci A, Castiello C, Mai A, Zwergel C, Valente S. Heterocycles–Containing HDAC Inhibitors Active in Cancer: An Overview of the Last Fifteen Years. ChemMedChem. 2024; Aug 29,1-53; Available from: doi.org/10.1002/cmdc.202400194
- Kostas Palamaris, Myrto Moutafi, Hariklia Gakiopoulou, Stamatios Theocharis. Histone Deacetylase (HDAC) Inhibitors: A Promising Weapon to Tackle Therapy Resistance in Melanoma. International Journal of Molecular Sciences. 2022; Mar 27;23(7):3660-3680.Available from: https://doi.org/10.3390/ijms23073660
- Tímár J, Ladányi A. Molecular Pathology of Skin Melanoma: Epidemiology, Differential Diagnostics, Prognosis and Therapy Prediction. International Journal of Molecular Sciences. 2022; May 11;23(10):5384. Available from: https://doi.org/10.3390/ijms23105384

- Topalian SL, Taube JM, Anders RA, Pardoll DM. Mechanism-driven biomarkers to guide immune checkpoint blockade in cancer therapy. Nature Reviews Cancer. 2016; Apr 15;16(5):275–287. Available from: doi:10.1038/nrc.2016.36.
- Vlasiou M. In Silico Techniques Used for Evaluation of Anticancer Metal- Based Compounds. Anti-Cancer Agents in Medicinal Chemistry. 2022; Aug 2;22. Available from: DOI: https://doi.org/10.2174/1871520622666220802145433
- Nur Halimatus Saadiah Abdullah1 , Lailatun Nazirah Ozair1*, Bohari Mohd Yamin.A short review on the synthesis of azamacrocyclic ligand: conventional and non-template methods, Malaysian Journal of Analytical Sciences, 2021; 25 (4) : 547 - 560
- Yang H, Lou C, Sun L, Li J, Cai Y, Wang Z, et al. admetSAR 2.0: web-service for prediction and optimization of chemical ADMET properties. Wren J, editor. Bioinformatics. 2018; Aug 28;35(6):1067–1069. Available from: doi: 10.1093/bioinformatics/bty707
- Aqra FMAM, Shah SA, Jamhour RMAQ, Siddiqi KS, Al-Jowder O, Al-Saleh F. Transition Metal Complexes of a New 12-Membered Tetraaza Macrocycle. Synthesis and Reactivity in Inorganic and Metal-Organic Chemistry. 1994; Nov;24(9):1599–1612. Available from: http://dx.doi.org/10.1080/00945719408002583
- AYİPO Y, OSUNNİRAN W, BADEGGİ U, SAHEED I, JIMOH A, BABAMALE H. Synthesis, characterization and antibacterial study of Co(II) and Cu(II) complexes of mixed ligands of piperaquine and diclofenac. Journal of the Turkish Chemical Society Section A: Chemistry. 2021; May 31;8(2):633–50.Available from: DOI: https://doi.org/ 10.18596/jotcsa. 898523.
- Chandra S, Smriti Raizada, Rani S. Structural and spectral studies of palladium(II) and platinum(II) complexes derived from N,N,N,N-tetradentate macrocyclic ligands. Spectrochimica Acta Part A: Molecular and Biomolecular Spectroscopy. 2008; Nov 1;71(2):720–4. Available from: doi:10.1016/j.saa.2007.12.051
- Swamy SJ, Pola S. Spectroscopic studies on Co(II), Ni(II), Cu(II) and Zn(II) complexes with a N4-macrocylic ligands. Spectrochimica Acta Part A: Molecular and Biomolecular Spectroscopy. 2008; Sep;70(4):929–933. Available from: doi:10.1016/j.saa.2007.11.005
- Gupta LK, Chandra S. Spectroscopic characterization and EPR spectral studies on transition metal complexes with a novel tetradentate, 12-membered macrocyclic ligand. Spectrochimica Acta Part A Molecular and Biomolecular Spectroscopy. 2006; Mar 10;65(3-4):792–796. Available from: doi:10.1016/j.saa.2005.12.042
- Carrasco R, Cano J, Ottenwaelder X, Aukauloo A, Journaux Y, Ruiz-García R. Molecular and electronic structure of square-planar nickel(ii), nickel(iii) and nickel(iii)π-cation radical complexes with a tetradentate o-phenylenedioxamidate redox-active ligand. Dalton Transactions. 2005;(15):2527. Available from: DOI : 10.1039/b502481a
- Chagas, C. M., Moss, S., & Alisaraie, L.. Drug metabolites and their effects on the development of adverse reactions: Revisiting Lipinski's Rule of Five. International Journal of Pharmaceutics, 2018; 549, 133-149,1-2. Available from: https://doi.org/10.1016/j.ijpharm.2018.07.046
- Stienstra K, Ieritano C, Haack A, W. Scott Hopkins. Bridging the Gap between Differential Mobility, Log *S*, and Log *P* Using Machine Learning and SHAP Analysis. Analytical chemistry. 2023; Jun 29;95(27):10309–10321. Available from: https://doi.org/10.1021/acs.analchem.3c00921
- Giang Huong Ta, Cin-Syong Jhang, Weng CF, Leong MK. Development of a Hierarchical Support Vector Regression-Based In Silico Model for Caco-2 Permeability. Pharmaceutics. 2021; Jan 28;13(2):174–4. Available from: https://doi.org/10.3390/pharmaceutics 13020174
- Storelli F, Olena Anoshchenko, Unadkat JD. Successful Prediction of Human Steady-State Unbound Brain-to-Plasma Concentration Ratio of P-gp Substrates Using the Proteomics-Informed Relative Expression Factor Approach. Clinical Pharmacology & Therapeutics. 2021; Mar 6;110(2):432–442, Available from: https://doi.org/10.1002/cpt.2227
- Das A, Rai J, Roth MO, Shu Y, Medina ML, Barakat MR, et al. Coupled catalytic states and the role of metal coordination in Cas9. Nature Catalysis [Internet]. 2023; Oct 1 [cited 2023; Nov 3];6(10):969–977. Available from: https://www.nature.com/articles/s41929-023-01031-1
  Available from: https://doi.org/10.1038/s41929-023-01031-1
- Ahmed, Elzupir AO, Abou-Krisha MM, Yousef TA. New Dual Inhibitors of SARS-CoV-2 Based on Metal Complexes with Schiff-Base 4-Chloro-3-Methyl Phenyl Hydrazine: Synthesis, DFT, Antibacterial Properties and Molecular Docking Studies. Inorganics (Basel). 2023; Jan 29;11(2):63. Available from: https://doi.org/10.3390/inorganics11020063
- Guechtouli N, Zaater S, Kichou N, Bouaziz-Terrachet S, Meghezzi H. Theoretical investigation of dicarboxamide mono copper (II) and novel transition metal complexes: Structural, chemical reactivity, vibrational and in-silico biological analysis. Journal of Molecular Structure. 2019; Jul;1188:23–30. Available from: https://doi.org/10.1016/j.molstruc.2019.03.068
- Saleh AL-Ghamdi. Structural and biological investigations of Fe(III) and Co(II) complexes with tryptophan and 2,2'-bipyridine: implications for antibacterial and antifungal applications. Journal of Umm Al-Qura University for Applied Sciences. 2025; Mar 3. Available from: https://doi.org/10.1007/s43994-025-00215-8
- Dhelal Ayad Shaker, Haider Abbas Mahdi, Synthesis and Spectral Identification of Some New Schiff Base Compounds: A HOMO-LUMO Study of Frontier Molecular Orbitals, Advanced Journal of Chemistry, Section A, 2025; 8(5), 835-844.Available from: https://doi.org/10.48309/ajca.2025.476161.1663
- Akbari Z, Stagno C, Iraci N, Efferth T, Omer EA, Piperno A, et al. Biological evaluation, DFT, MEP, HOMO-LUMO analysis and ensemble docking studies of Zn(II) complexes of bidentate and tetradentate Schiff base ligands as antileukemia agents. Journal of Molecular Structure. 2024; Apr; 1301:137400.Available from: https://doi.org/10.1016/j.molstruc.2023.137400
- Sandhu Q, Pervaiz M, Majid A, Younas U, Saeed Z, Ashraf A, et al. Review: Schiff base metal complexes as anti-inflammatory agents. Journal of Coordination Chemistry. 2023; May 19;76(9-10):1094–1118. Available from: https://doi.org/10.1080/00958972.2023.2226794
- Subhash, Chaudhary A, Jyoti, Kumar M, Mamta, Solanki R. Synthesis, structural elucidation, DFT investigations, biological evaluation and molecular docking studies of tetraamide-based macrocyclic cobalt (II) complexes. Journal of the Iranian Chemical Society. 2023; Jul 4;20(9):2339–62. Available from: https://doi.org/10.1007/s13738-023-02847-1
- Muhammad, Araby A, Walla Alelwani, Kattan SW, Mansouri OA, Rasib M, et al. Green-synthesized nanoparticles of the polyherbal extract attenuate the necrosis of pancreatic ß-cell in a streptozotocin-induced diabetic model. Heliyon. 2023; May 1;9(5):e16137–7, Available from: doi.org/10.1016/j.heliyon.2023.e16137

- Kumar P, Nagarajan A, Uchil PD. Analysis of Cell Viability by the MTT Assay. Cold Spring Harbor Protocols [Internet]. 2018; Jun;2018(6):pdb.prot095505. Available from: https://pubmed.ncbi.nlm.nih.gov/29858338/
- Sathiya Kamatchi T, Mohamed Subarkhan MK, Ramesh R, Wang H, Małecki JG. Investigation into antiproliferative activity and apoptosis mechanism of new arene Ru(ii) carbazole-based hydrazone complexes. Dalton Transactions. 2020;49(32):11385–11395. Available from: DOI: 10.1039/d0dt01476a.